

Fig. 3 Head-on collision of two shock waves.

right ( $x = 60$ ) ends as shown in Fig. 2. The movement  $\delta$  given to the particle at the left end is

$$\delta = \frac{\Delta x}{2} \left( 1 - \cos \frac{2\pi}{30} i \right) \quad i = 1, \dots, 15 \quad (13)$$

where  $i$  indicates the time  $t = i\Delta t$  and  $\delta = \Delta x$  when  $i \geq 16$ . The movement of the particle at the right end is given by  $-\delta$ . As a result of these movements, two waves are generated. In other words, a finite slope of the density distribution is created by the movements added to the particles at the ends so that finite acceleration given by Eq. (11) is induced on the rest of the particles. Consequently, the density variation, i.e.,  $(\rho - \rho_0)/\rho_0$ , of amplitude 0.125 travels from one particle to another, although each particle moves slightly around the initial position.

As depicted by the loci of the waves in Fig. 2 (indicated by dash-dotted lines), the two waves created at the ends travel at a constant speed toward the opposite ends. The waves merge at the center of the  $x$  axis, at around time 36. At this time, the amplitude of the waves is doubled, and the distance between the particles at the center becomes the smallest. After this, the wave separates into the original waves, and they travel to opposite ends. As can be observed, this collision does not affect the shape of the waves or the speed at which they travel.

### C. Equation for a Compressible Fluid with the Diffusion Term

In this section, we consider application of the particle method to the equation for finite waves with the diffusion term, Eq. (9). At time  $t = -50$ , the particles are placed at a distance of  $0.8\Delta x$  apart for  $-80 \leq x \leq -20$ ,  $1.0\Delta x$  apart for  $-20 \leq x \leq 60$ , and  $0.6\Delta x$  apart for  $60 \leq x \leq 120$  (Fig. 3). As a result, the density distribution is discontinuous. The variation of the density distribution  $(\rho - \rho_0)/\rho_0$  is depicted by a solid line. The dashed line and the dash-dotted line indicate the particle velocity and the locus of the shock wave, respectively. The values of the other parameters used in this calculation are  $\nu(\Delta t/\Delta x^2) = 0.5$ ,  $\nu/(a_0\Delta x) = 5.0$ ,  $\Delta x/\sigma = 1.0$ , and  $\gamma = 1.4$ . As shown in Fig. 3, the particles accelerated according to Eq. (12) generate a head-on collision of two shock waves of different magnitude. The shapes of the shock waves vary when the two waves are merged; however, they recover after separation. Because of this collision, the velocity of the shock wave traveling to the right changes from  $U^+/a_0 = 1.07$  to 0.85 and the velocity of the shock wave traveling to the left changes from  $U^-/a_0 = -1.16$  to  $-1.07$ . These values agree with the analytic solutions.<sup>6,7</sup>

## IV. Conclusion

A grid-free numerical method is presented for solving the equations of compressible fluids by using the particle model.

This model is used to simulate numerically the time-dependent one-dimensional phenomena that arise by solving the linear wave equation, the Burgers equation, and the equation for compressible fluids, both with and without the diffusion term. The formation of the steady shock wave and the interactions of the linear waves and of the nonlinear shock waves are successfully simulated by our method. The ability of the method to treat the compressibility has been adequately shown. As far as we know, this is the first successful simulation of the compressible fluids by the particle scheme.

## References

- Hockney, R. W., and Eastwood, J. W., *Computer Simulation Using Particles*, McGraw-Hill, New York, 1980, p. 2.
- Spalart, P. R., Leonard, A., and Baganoff, D., "Numerical Simulation of Separated Flows," NASA TM-84328, 1983, p. 12.
- Ogami, Y., and Akamatsu, T., "Viscous Simulation Using the Particle Method—the Diffusion Velocity Method," *Computers and Fluids*, Vol. 19, No. 3/4, 1991, p. 433.
- Chorin, A. J., "Numerical Study of Slightly Viscous Flows," *Journal of Fluid Mechanics*, Vol. 57, Pt. 4, 1973, p. 785.
- Van Rosseel, H. J., and Hui, W. H., "Unsteady Three-Dimensional Newton-Busemann Flow Using Material Functions," *Journal of Non-Linear Mechanics*, Vol. 26, No. 1, 1983, p. 73.
- Tatsumi, T., "Fluid Dynamics" (in Japanese), *Baihuukan*, 1983, p. 205.
- Tatsumi, T., and Tokunaga, H., "One-Dimensional Shock Turbulence in a Compressible Fluid," *Journal of Fluid Mechanics*, Vol. 65, Pt. 3, 1974, p. 581.

## Vortex-Induced Energy Separation in Shear Flows

J. J. O'Callaghan\* and M. Kurosaka†

University of Washington, Seattle, Washington 98195

### I. Introduction

ONE of the interesting features of unsteady aerodynamics is its wealth of counterintuitive phenomena. An excellent example of these is that of energy separation in a flow, where regions of high and low energy can be identified in the flowfield. A measure of the energy of the flow is the total temperature  $T_t$ .

In adiabatic, inviscid flows that do no mechanical shaft work, we are used to thinking of the total temperature as being constant, since the energy of the flow is conserved. However,  $T_t$  is constant along a streamline only for steady flows; in unsteady flows, the  $T_t$  along the fluid particle trajectory can vary significantly. This phenomenon is reflected in the following energy equation:

$$C_p \frac{DT_t}{Dt} = \frac{1}{\rho} \frac{\partial p}{\partial t} \quad (1)$$

We see that if the flow is steady, then the  $T_t$  is constant along the streamline; but if an unsteady pressure field is imposed on the flow, then the  $T_t$  of the flow can change both in space and time. In the latter case, we can say that the energy of the flow becomes separated; some regions of the flowfield contain more energy than others.

Presented as Paper 92-0192 at the AIAA 30th Aerospace Sciences Meeting, Reno, NV, Jan. 6-9, 1992; received April 14, 1992; revision received Oct. 23, 1992; accepted for publication Nov. 5, 1992. Copyright © 1992 by the American Institute of Aeronautics and Astronautics, Inc. All rights reserved.

\*Graduate Student, Department of Aeronautics and Astronautics; currently, Stability and Control Engineer, Renton Aerodynamic Division, Boeing Commercial Airplane Company, Renton, WA.

†Professor, Department of Aeronautics and Astronautics. Associate Fellow AIAA.

Energy separation has been observed in the wakes of circular cylinders<sup>1</sup> and in free and impinging jets.<sup>2</sup> Kurosaka et al.<sup>1</sup> and Fox et al.<sup>2</sup> have suggested that the energy separation in these flows is produced by the unsteady static pressure fields associated with the vortical structures that dominate the flows. Although the mechanism of vortex-induced energy separation predicts the nonuniform  $T_t$  distributions in these flows adequately, the flows themselves are complicated by other extraneous factors, such as three dimensionality and counter-rotating vortical structures that may affect energy separation.

The purpose of this research is to confirm the mechanism of vortex-induced energy separation in the simplest context, i.e., to study  $T_t$  distribution in a flow that can be modeled by a row of vortices convecting downstream in an otherwise uniform flow. Such a flow can be approximated by a shear layer, in which vortical structures are convected downstream between two uniform streams. The shear layer contains the essential features of wake and jet flows as far as energy separation is concerned—large, convecting vortical structures—but lacks the complicated three dimensionality of wakes and jets. In this experiment, we create shear layers by inserting a wire mesh screen or a plate normal to a uniform flow in a wind tunnel; the velocity gradient behind these obstructions causes a shear layer to be shed from the screen or plate tip.

## II. Experiments

### A. Experimental Apparatus

The experiments were performed in an existing blow-down wind-tunnel facility described in Refs. 1 and 2, modified to fit a new square test section of  $8.9 \times 8.9$  cm and 50 cm in length, which exits to room air.

The test section walls are made of Plexiglas to minimize thermal conduction, which can contaminate near-surface temperature measurements. Holes in the tunnel ceiling provide access for a total temperature and total pressure probe to traverse the test section vertically and obtain measurements at various distances from the tunnel floor. In the screen tests, a screen that spans half the height of the tunnel is placed at the test section entrance. In the flat plate tests, this screen was replaced by a solid plate that was set to extend 0.64, 1.27, 1.90, and 2.54 cm into the test section.

Prior to the main test, a check-out test for the uniform flow (without any physical objects within the tunnel) was conducted to establish the baseline condition; the distributions of the total pressure and temperature were confirmed to be those of the standard turbulent boundary layer. For these and other details see Ref. 3.

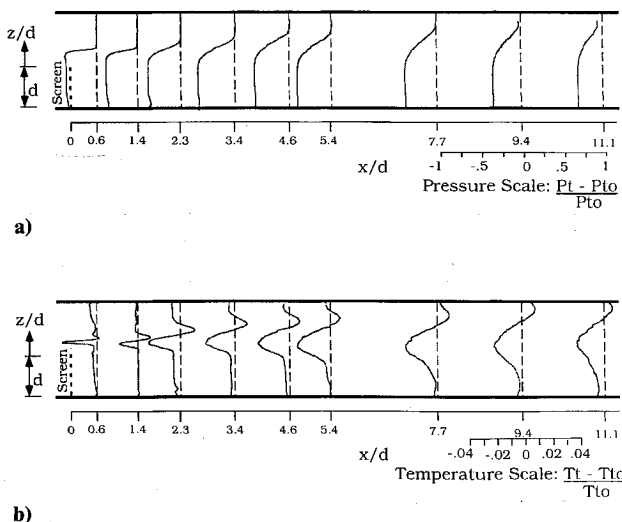


Fig. 1 Profiles behind screen: a) total pressure,  $P_{t0} = 168$  kPa;  $T_{t0} = 293$  K and b) total temperature,  $P_{t0} = 168$  kPa;  $T_{t0} = 293$  K.

### B. Results 1: Screen

Figure 1a shows the total pressure  $P_t$  and Fig. 1b total temperature  $T_t$  profiles corresponding to the settling chamber pressure  $P_{t0}$  of 168 kPa and temperature  $T_{t0}$  of 293 K.

The growth of the shear layer from the top of the screen is evident from the  $P_t$  profiles. Note that at  $x/d = 0.6$  it appears that the shear layer lies slightly above the top of the screen; this suggests that the shear layer curves upward from the screen tip as part of the flow ahead of the screen accelerates over the top of the screen instead of passing directly through it. Farther downstream, the layer straightens and flows parallel to the walls, though its original curvature has shifted it above the vertical centerline of the tunnel. As the layer spreads downstream, the velocity gradient across it becomes less severe, and  $P_t$  in the high-speed stream decays in the downstream direction.  $P_t$  in the slower stream increases downstream; at  $P_{t0} = 168$  kPa,  $P_t - P_{t0} = -78$  kPa in the slow stream at  $x/d = 0.6$  and  $z/d = -0.5$ , but  $P_t - P_{t0} = -65$  kPa in that stream at  $x/d = 11.1$  and at the same  $z/d$ . The shear layer stops spreading upward at about  $x/d = 7.7$  as the tunnel ceiling starts to interfere with the flow. However, the off-center position of the layer gives it room to spread downward and toward the tunnel floor even at large  $x/d$ .

The  $T_t$  profiles of Fig. 1b confirm the mechanism of vortex-induced energy separation, as is evident from the following observations.

- 1) The energy separation region encloses the shear layer and grows with it, suggesting strongly that this region is the result of the vortex structures which make up the shear layer.
- 2)  $T_t$  increases on the upper side of the vortices where the velocities induced by the shear layer vortices coincide with the freestream motion and decreases on the lower side where these velocities oppose the freestream motion (see Refs. 1 and 2; the

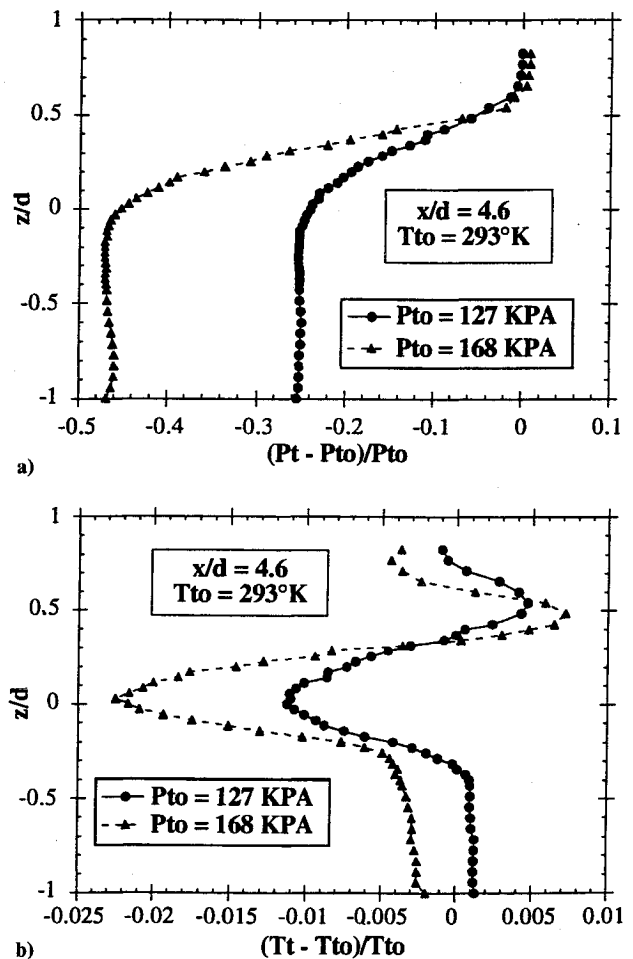


Fig. 2  $T_t$  and  $P_t$  profiles behind the screen at  $x/d = 4.6$  and  $P_{t0} = 127$  and 168 kPa: a)  $P_t$  profiles and b)  $T_t$  profiles.

vortices generated in the shear layer rotate clockwise in the view taken for the present).

3) The magnitudes of heating and cooling are comparable. However, the nonuniformity of the shear-layer flow results in more cooling than heating. For instance, at  $x/d = 4.6$ , the maximum heating is  $2^\circ\text{C}$ , although the maximum cooling is  $7^\circ\text{C}$ . This can be observed more easily in Fig. 2.

4) The results corresponding to different  $P_{00}$  show that the  $T_i$  separation is roughly proportional to the square of the difference  $\Delta M$  in the Mach numbers between the fast and slow streams.<sup>3</sup> For example, Fig. 2 shows that there is  $3^\circ\text{C}$  of cooling and  $1^\circ\text{C}$  of heating at  $P_{00} = 127$  kPa where  $\Delta M = 0.55$ , compared to  $7^\circ\text{C}$  of cooling and  $2^\circ\text{C}$  of heating at  $P_{00} = 168$  kPa where  $\Delta M = 0.82$ . Thus, the square of the difference between the Mach number is  $(0.82/0.55)^2 = 2.2$ , which compares favorably with the corresponding ratios for heating and cooling.

### C. Results 2: Flat Plates

Figure 3 obtained for  $h = 1.27$  cm is typical for the flat-plate results. Notice that each of the plots contains a "forward-facing probe" curve and a "backward-facing probe" curve. The total temperature and total pressure probe used in this experiment only reads accurately when it faces the oncoming air; i.e., the air must be blowing into the probe to get good data. However, a recirculation zone exists behind the plate, where some of the air may actually be moving upstream, that is, toward the tunnel inlet (see, e.g., Ref. 4 for a similar flow behind a backward-facing step). To correctly measure  $T_i$  and  $P_i$  of upstream-flowing air in the recirculation region, the probe must face downstream, toward the tunnel exit. At some point between the tunnel floor and the top of the shear layer shed from the plate tip, the air reverses direction from upstream flow to downstream flow; at this point, the velocity

should be zero and the  $T_i$  and  $P_i$  measured by both an upstream-facing probe and a downstream-facing probe should be the same. The results shown in Fig. 3, indeed, show such an intersection between the backward- and forward-facing probe data somewhere between the tunnel floor and the plate tip. Above this intersection, the air flows downstream and we expect the forward-facing probe data to be valid; below the intersection, the air flows upstream and we expect the backward-facing probe data to be valid.

From Fig. 3b, the presence of the total temperature separation is again easily observed. Compared to the screen tests, the amount of cooling is larger. This is due to the recycling of the air trapped in the recirculation zone where it is repeatedly subjected to the cooling effects of the vortices. Therefore, the dependence on the Mach number is more complicated here than in the screen tests.

Plate height does not appear to have much effect on the magnitude of temperature separation, as long as the plate is high enough for the shear layer and its vortices to develop.

### III. Conclusions

The results obtained in this experiment are consistent with, and are predicted by, the mechanism of vortex-induced energy separation. As expected, the  $T_i$  of the flow increases in a region where the vortex-induced velocities coincide with the freestream motion, and decreases where these velocities oppose the freestream motion. The greater cooling in the slow stream of the shear layer is explainable as the result of the velocity gradient through the shear layer. The extent of the energy separation region coincides with the location of the vortex structures, leaving no doubt that the two are intimately linked. The energy separation increases as the severity of the shear layer generating the vortices increases; the energy separation is, in general, roughly proportional to the square of the difference in Mach number between the shear layer's fast and slow streams.

Given this evidence, we can conclude that the mechanism of vortex-induced energy separation is real and correct. Energy separation and unsteady vortical structures are inseparable phenomena;  $T_i$  separation will always exist to some degree whenever unsteady vortical structures are present. This fact can be used to detect the presence of unsteady vortices by point measurements, using a conventional  $T_i$  probe: a nonuniform  $T_i$  distribution indicates a region of separated flow or another kind of flow in which unsteady vortices are found.

### Acknowledgment

This research is supported by the Air Force Office of Scientific Research under Contract F49620-88-0041. The authors wish to acknowledge the suggestions made by M. F. Platzer of the Naval Postgraduate School and the skillful assistance received from R. A. Blair in conducting the experiments.

### References

- Kurosaka, M., Gertz, J. B., Graham, J. E., Goodman, J. R., Sundaram, P., Riner, W. C., Kuroda, H., and Hankey, W. L., "Energy Separation in a Vortex Street," *Journal of Fluid Mechanics*, Vol. 178, May 1987, pp. 1-29.
- Fox, D. M., Kurosaka, M., and Hirano, K., "Total Temperature Separation in Jets," AIAA Paper 90-1621, June 1990; also Fox, M. D., Kurosaka, M., Hedges, L., and Hirano, K., "The Influence of Vortical Structures on the Thermal Fields of Jets," *Journal of Fluid Mechanics* (to be published).
- O'Callaghan, J. J. "Vortex-Induced Energy Separation in Shear Flows," M.S. Thesis, Dept. of Aeronautics and Astronautics, Univ. of Washington, Seattle, WA, 1991.
- Pronchik, S. W., and Kline, S. J., "An Experimental Investigation of the Structure of a Turbulent Reattaching Flow Behind a Backward-Facing Step," Thermosciences Div., Dept. of Mechanical Engineering, Stanford Univ., Rept. MD-42, Stanford, CA, 1983.

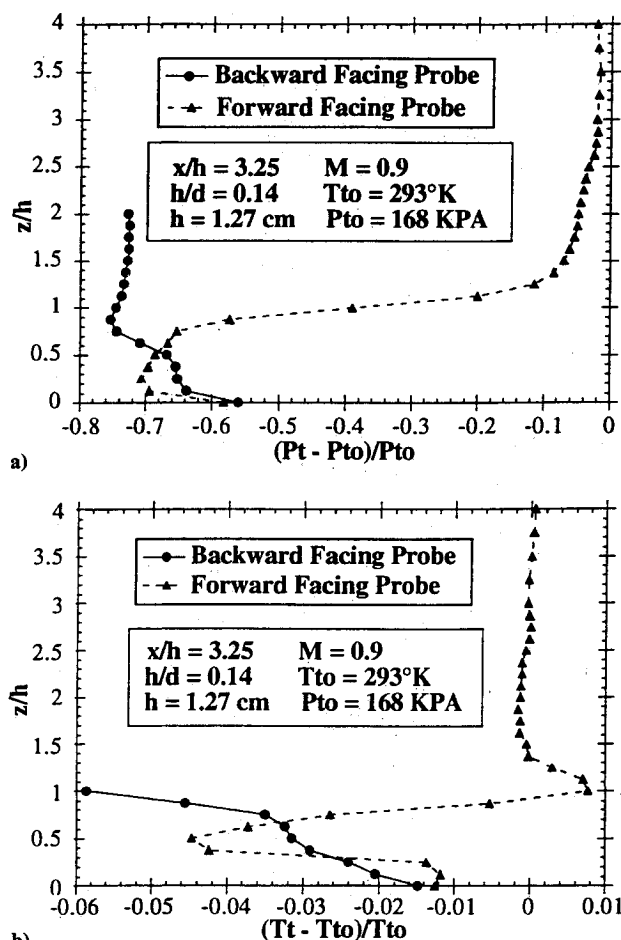


Fig. 3  $T_i$  and  $P_i$  profiles behind 1.27-cm plate at  $M = 0.9$  and  $x/h = 3.25$ : a)  $P_i$  profile and b)  $T_i$  profile.